The Effect of Impact Angle on the Secondary Droplets at High Impact Velocity

David A. Burzynski*, Stephan E. Bansmer
Technische Universität Braunschweig, Institute of Fluid Mechanics, Braunschweig, Germany
*Corresponding author: d.burzynski@tu-bs.de

Abstract
This study focuses on the secondary droplets ejected during splashing at different impact angles. We consider the theory of Riboux & Gordillo [1], which attributes the generation of secondary droplets to a lift force that acts on the spreading lamella, and propose a new approach to handle the oblique impact. This approach is based on previous studies on the lamella formed by impinging jets, where the impacting flow is distributed in the azimuthal direction. To validate the proposed method, we used a flywheel experiment and captured the secondary droplets that are ejected at Weber number larger than 4500 at three different impact angles. In our experimental setup, the droplets were formed by a droplet generator and then let to fall freely due to gravity until impacting the substrate, which was mounted on a flywheel. The small and fast secondary droplets were captured using a shadowgraph technique together with a high-resolution camera and Nd:YAG laser with diffuser optics. The experimental results showed an acceptable agreement with the prediction made by our method in all studied cases. We demonstrate that the shape and droplet size distribution are affected by the impact angle, while the velocity of the ejected droplets remains constant in the azimuthal direction.

Keywords
splashing modeling, oblique impact, high Weber numbers, secondary droplets, size and velocity distributions.

Introduction

When a droplet impacts on oblique surfaces at high velocity and under atmospheric pressure conditions, a part of the droplet's mass sticks on the surface, forming a lamella. The other part of the mass atomizes in the early stage of the impact into small secondary droplets. This phenomenon, which is known as splashing, is important in many technical applications, such as aircraft icing, gas turbines, or vehicle soiling [2]. In the case of in-flight aircraft icing, the splashing occurs when supercooled large water droplets impact the aircraft. These droplets are formed in clouds due to the melting of snow or the coalescence of smaller droplets. After the collision, the mass stuck on the surface eventually freezes and the process of ice accretion starts. The ejected secondary droplets are likely to be transported by the airflow and impact other components located downstream from the first impact position. The aircraft icing can be extremely hazardous and cause many fatal events in aviation, such as the crash of Embraer EMB-500 on December 8, 2014 [3]. To understand what is happening under these extreme situations, the dynamics of both the deposit mass and the secondary droplets must be studied under similar conditions. However, since the freezing process starts at the final stage of impact, experiments at room temperature are suitable to investigate the dynamics of secondary droplet generation [4].

Despite decades of studies on droplet impact on dry surfaces, only a handful of studies have been published on oblique impacts. The main characteristic of this kind of impacts is the formation of an asymmetric spreading lamella [5]. When the impact angle is reduced below 35°, the dynamics of the deposited mass changes from deposition to rebound [6]. More precisely, a threshold angle of 30° has been found for these changes in the dynamics during the impact [7]. It has also been observed that the splashing at moderate velocity impact can be completely suppressed for angles smaller than the threshold angle [8]. Although these studies concentrated on the impact at a relatively low impact velocity, several similarities in the outcome have been observed at high impact velocity [4, 9] It has been observed that the generation of secondary droplets depends on the impact angle and that the amount of droplets generated changes in the azimuthal direction [4]. However, this conclusion was made by the author after observing the ejection of a single droplet for the impact at 0°. This was a particular case, but normally the splash produces a large number of secondary droplets [10]. Nevertheless, almost nothing is known about these secondary droplets.

Experiments performed with smooth and textured surfaces at different angles demonstrate the significant role that the aerodynamic forces play in the splashing process [9]. The impact on textured surfaces forms a symmetrical distribution of secondary droplets almost independently of the impact angle, which suggests that surrounding gas escapes through the texture, thus reducing the effect of the tangential velocity. The effect of the surrounding gas on splashing has been demonstrated in several studies showing that even splashing can be suppressed by reducing the gas pressure [2]. A recent theory developed by Riboux & Gordillo [1] that takes into account gas and liquid effects has shown a good agreement with a large number of experiments; however, the theory has been proposed for the impact normal to the surface. One solution to address the oblique impact in this theory was proposed in accordance with the analysis of moving surfaces [8]; however, the outcome of a droplet impacting on a moving surface and the stationary oblique impact are not necessarily the same [11]. Therefore, it is still uncertain whether the use of a moving surface model is suitable for a rough estimation in the oblique impact case.

https://doi.org/10.24355/dbbs.084-201909121447-0

In this study, we analyze the ejected secondary droplets to understand how the impact angle affects the splashing. The first part focuses on the mechanism responsible for the generation of secondary droplets from a theoretical point of view. Here, we propose a new approach to handle the oblique impact using the theory of Riboux & Gordillo. In the second part, we test this method by measuring the droplet size and velocity and comparing the results with the predictions. We demonstrate that the diameter and velocity of the secondary droplets ejected at high impact velocity can be predicted using our approach.

Experimental method

A droplet generator was used to form and release distilled water and ethanol droplets of $D_{H_2O} = 3.4$ mm and $D_{Eth} = 2.8$ mm. They fall due to gravity until they impact with the substrate mounted on a rotating flywheel. Fig. 1 shows a schematic representation of this experiment. The impact velocity U is defined as the relative velocity between the droplet and the flywheel. It was set to $U \approx 10.2$ m/s for the experiment with water and from $U \approx 7$ m/s to $U \approx 10$ m/s for the experiment with ethanol. The experiments were conducted at ambient conditions $T_0 = 20$ °C and $p_0 = 1$ bar; the properties of the liquids are summarized in Table 1. This setup allows us to study the impact in a range from $\mathrm{We} = \rho_{liq} U^2 D/\sigma_{liq,g} \approx 4900$ to 9800 and $\mathrm{Re} = \rho_{liq} U D/\mu_{liq} \approx 12500$ to 34500. Three different impact angles $\theta = 90°$, $60°$ and $45°$ were investigated by changing the substrate holder. Glass with a roughness of $R_a = 22$ nm and $R_z = 198$ nm was used as the impact surface. A detailed explanation of the components and the mode of operation of the flywheel experiment can be found in our previous investigation [12].

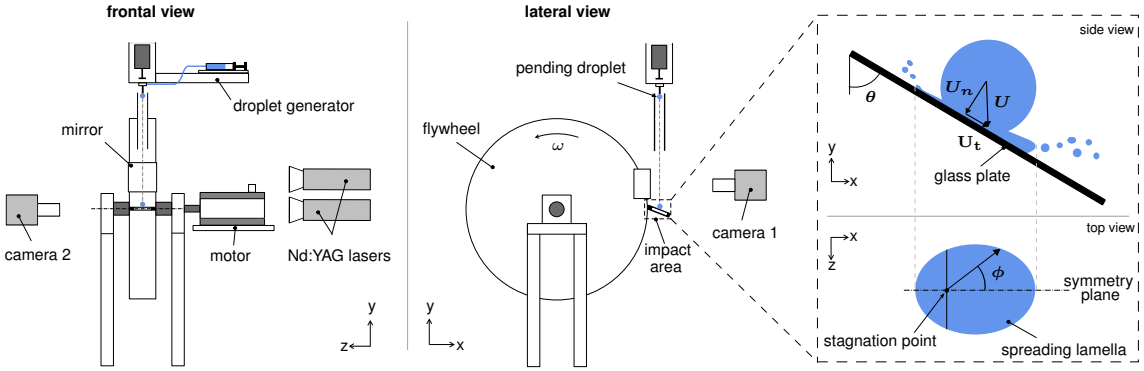

Figure 1. Experimental setup. The frontal and lateral views show the main components of the experiment and demonstrate its mode of operation. The recording system consists of two high-resolution cameras and two lasers with diffuser optics, which capture the droplet before (camera 1) and during impact (camera 2). The schematic representation of an impacting droplet shows the generation of secondary droplets, the impact (θ) and azimuthal (ϕ) angle definitions, and the velocity components (U,U_n,U_t).

The splashing was observed using a shadowgraph technique with two double-frame CCD cameras with a resolution of 4008×2672 pixel together with two Nd:YAG lasers with diffuser optics. The first camera captured the droplet before the impact, allowing a precise estimation of the impact conditions. The second camera captured the secondary droplets as shown in Fig. 1. The resolution of this camera was 12 µm/px, which allowed to detect droplets with a minimum diameter of 36 µm. The synchronization of the cameras with the droplet generator and flywheel was done using a delay generator. The trigger signal was generated by a light barrier mounted on the flywheel.

Table 1. Properties of the liquids.

	density ρ_{liq} (kg/m^3)	viscosity μ_{liq} (Pas)	surface tension $\sigma_{liq,g}$ (N/m)
distilled water	998	1.002×10^{-3}	72.75×10^{-3}
ethanol	790	1.24×10^{-3}	22.55×10^{-3}

Observations and modeling

Two different splashing behaviors were observed by changing the drop liquid: A prompt splash, where the droplets are generated directly from the rim spreading over the surface, and a corona splash, where the droplets are formed at the rim of the levitating lamella (see Fig. 2). While prompt splash was observed for the water droplets ($\mathrm{Oh} = \mu_{liq}/(\sqrt{\rho_{liq} D \sigma_{liq,g}}) \approx 0.002$), the corona splash was observed only when ethanol droplets impacted with the surface ($\mathrm{Oh} \approx 0.006$). Roisman et al. [13] elaborated a map presented by Palacios et al. [14] for high Weber and Reynolds numbers, separating the deposition, corona, and prompt splash. They established that $\mathrm{Oh} = 0.0044$ is the threshold that separates the different splashes at high impact velocity, which is in agreement with our observations. These two splashing phenomena should be considered separately because of the different way they affect for secondary droplet generation. Although we focus our analysis on the prompt splash, we still provide the most relevant insights into the corona splash.

https://doi.org/10.24355/dbbs.084-201909121447-0

Fig. 2 demonstrates the asymmetrical behavior of splashing in relation to the impact on inclined surfaces. To analyze this phenomenon, the velocity vector (U) is commonly decomposed on its normal (U_n) and tangential (U_t) components (see Fig. 1). This analysis was carried out from a geometrical point of view and does not necessarily represent the velocity of the spreading lamella, which decelerates over time. The asymmetric secondary droplet distribution in azimuthal direction (ϕ) is attributed to the change in the tangential velocity at the initial stage of impact [6]. In the case of water droplets at $\theta = 45^\circ$, the splashing is suppressed in the upstream direction, while in the downstream direction the number of secondary droplets increases relative to the normal impact.

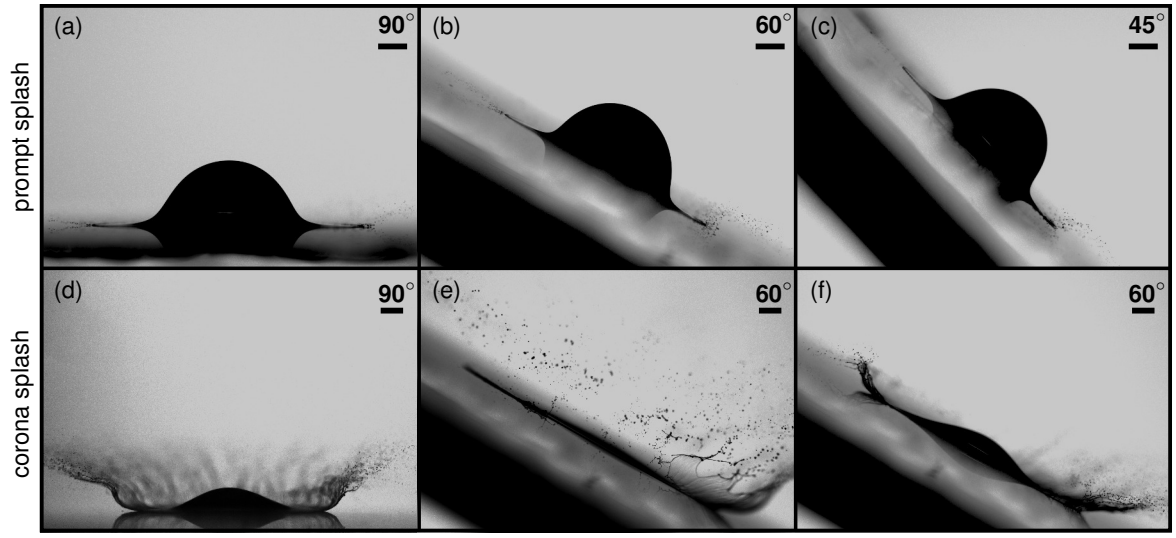

Figure 2. Droplets impacting at different angles θ and velocities. (a-c) show the effect of decreasing θ when water droplets impact at velocity $U \approx 10$ m/s ($\mathrm{We} \approx 4800$). (d-e) show the same configuration but using ethanol droplets at $U = 7$ m/s ($\mathrm{We} \approx 4800$). (e-f) show the effect of increasing the impact velocity up to $U \approx 10$ m/s ($\mathrm{We} \approx 9800$) but keeping θ constant. Scale bars 1 mm.

Is it possible to predict this behavior? Riboux & Gordillo [1] (hereafter RG) proposed a theory that predicts the splashing criterion in a simple way by using the properties of the fluid and the surrounding gas. They consider an inviscid and incompressible flow in their analysis and use the potential flow and lubrication theory to conclude that splashing occurs because of a lift force (F_L) acting upon the lamella. If the ratio of this lift force to surface tension

$$\beta = \sqrt{F_L / 2\sigma_{liq,g}}, \tag{1}$$

which is defined as the splashing parameter, is larger than 0.14, splash is expected. To estimate this lift force, it is necessary to calculate when the lamella separates from the surface (t_e); this is done using the RG expression

$$c_1 \mathrm{Re}^{-1} t_e^{-1/2} + \mathrm{Re}^{-2}\mathrm{Oh}^{-2} = c t_e^{3/2}, \tag{2}$$

where $c_1 = \sqrt{3}/2$, $c = 1.21$, $\mathrm{Re} = \rho_{liq} U_n R / \mu_{liq}$ and $\mathrm{Oh} = \mu_{liq} / (\sqrt{\rho_{liq} R \sigma_{liq,g}})$. This time is made dimensional as $T_e = t_e R / U_n$. The thickness and velocity of the lamella at the ejection time are defined as:

$$h_l = \frac{\sqrt{12} t_e^{3/2}}{\pi} \quad \text{and} \quad u_l = \frac{1}{2}\sqrt{\frac{3}{t_e}}, \tag{3a,b}$$

where the dimensional values are obtained as $H_l = h_l R$ and $U_l = u_l U_n$. Note that the quantities for the ejection time t_e, the lamella thickness h_l and velocity u_l are represented dimensionless to be consequent with the notation of Riboux & Gordillo. The lift force can then be calculated using the expression

$$F_L = K_{lub} \mu_g U_l + K_u \rho_g U_l^2 H_l, \tag{4}$$

where $K_{lub} \simeq -2(\ln(19.2\lambda/H_l) - \ln(1 + 19.2\lambda/H_l))$ is obtained from the lubrication theory and $K_u = 0.3$ is a numerically determined constant. In this way, the splashing threshold and the initial conditions of the ejected lamella can be calculated for a normal impact on dry surfaces.

To adapt these equations for the oblique impact, Hao et al. [8] proposed to add the geometrical tangential velocity U_t to Eq. 3b for times greater than T_e (hereafter Hao model). This assumption is based on the experiment of Bird et al. [15], where the droplet impacted normally on a moving surface. However, Zen et al. [16] carried out experiments analyzing the droplet impact on inclined and moving surfaces and remarked that the mechanism of the splashing is different in both cases. On a moving surface, the splash is promoted in the portion of fluid that moves opposite to the spreading lamella ($U_l - U_t$). The contrary is observed on the oblique impact ($U_l + U_t$). Another assumption made by Hao et al. [8] is that the lamella thickness has to remain constant in azimuthal direction, although the experiments of Šikalo et al. [6] show a thicker lamella in the downstream direction.

To predict the splashing in a more consistent way with the experiments, we propose the following method to handle the oblique impact. We assume inviscid and incompressible flow conditions as postulated by Riboux & Gordillo

https://doi.org/10.24355/dbbs.084-201909121447-0

[1]. This ideal flow condition assumes that the static pressure away from the stagnation point must be the same as the pressure of the surrounding gas. Thus, the Bernoulli equation states a constant flow velocity (see Fig.3). This method is also found in studies on the oblique impact of round jets [17, 18, 19], where an analytical solution has already been proposed to obtain the flux and thickness distribution in the azimuthal direction.

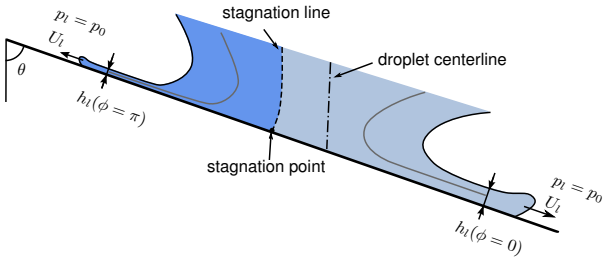

Figure 3. Schematic representation of a droplet impacting on an oblique solid surface. Dark blue area represents fraction of the flow carried in upstream direction. Gray lines illustrate the streamlines.

The similarities between the evolution of the spreading liquid from jets and droplets allow us to apply the expression for the normalized thickness distribution developed by Hasson & Peck [18], namely

$$h_{dist} \approx \frac{\sin^3\theta}{(1-\cos\phi\cos\theta)^2}. \tag{5}$$

At impact angles of $\theta = 90^\circ$, $h_f = 1$ so that lamella thickness is axisymmetric. By implementing this equation in the RG model, we obtained an expression that describes the azimuthal distribution of the lamella as a function of the impact angle. The rewritten equation 3a reads as follows:

$$H_l = \frac{h_{dist}\sqrt{12}t_e^{3/2}}{\pi}R. \tag{6}$$

Fig. 4 shows a comparison between the Hao model and our approach as a function of the impact angle for water droplets of $D = 3.4$ mm impacting at $U = 10$ m/s. The initial lamella thickness H_l is predicted by the Hao model to increase by decreasing the impact angle, though the lamella thickness is in all azimuthal directions the same. On the contrary, our model predicts a lower lamella thickness at the stagnation point $\phi = \pi/2$ and the upstream direction $\phi = \pi$ by decreasing the impact angle; at the same time, the lamella thickness increases in the downstream direction $\phi = 0$. The estimations made by our approach agree with the observations of Šikalo et al. [6].
The predicted velocity of the lamella U_l is more similar in both models, at least at higher impact angles. In fact, the velocity at $\phi = \pi/2$ is the same in both models; this is because the conservation of momentum in our analysis indicates that the velocity of the spreading lamella does not change in the azimuthal direction. Our approach also suggests that the velocity tends to zero the lower the impact angle is, therefore, at $\theta < 10$, $U_l \approx 0$ and the lamella may not form at all. The Hao model predicts in those cases that the entire liquid above the stagnation point $\pi/2 < \phi < \pi$ flows in the downstream direction; as a consequence, at the ejection moment the liquid has to flow downstream, whereupon the droplet would slip at the surface, avoiding any stagnation point. This has not been observed in the experiments, even when the velocity of a moving surface was higher than the droplet impact velocity $U_t >> U$ [20].
The splashing parameter β depends strongly on the calculated thickness and velocity; thus, the outcomes of the models are expected to differ from each other. Both models agree in the splash prediction at all azimuthal angles for

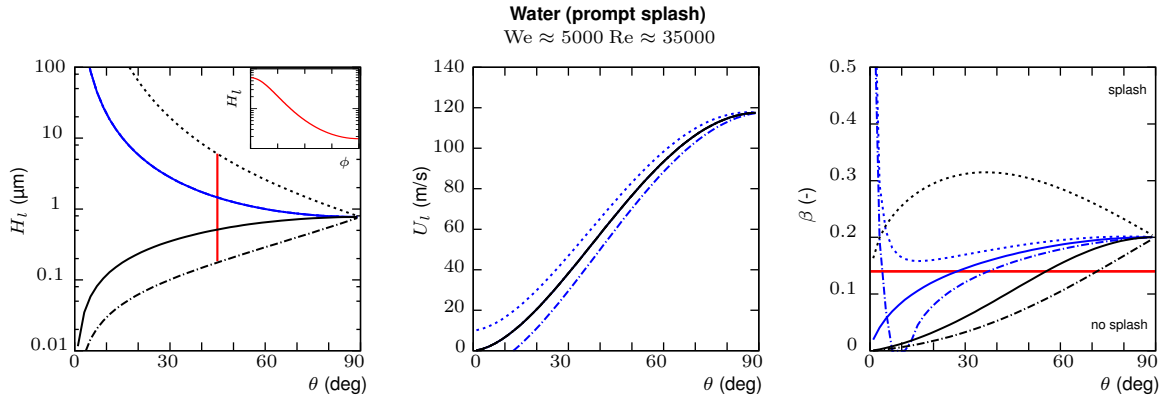

Figure 4. Analytical results of the lamella thickness H_l, its velocity U_l, and splashing parameter β. Black lines represent our model; blue lines represent the modified model presented by Hao et al. [8]. The upstream direction ($\phi = \pi$) is represented with dash-dotted lines, the stagnation point ($\phi = \pi/2$) with solid lines, and the downstream direction ($\phi = 0$) with dotted lines. The red line in H_t diagram shows the thickness as a function of ϕ for $\theta = 45^\circ$, in β diagram it indicates the splashing threshold $\beta = 0.14$.

https://doi.org/10.24355/dbbs.084-201909121447-0

high impact angles $\theta > 75^\circ$ and only at the downstream side $\phi = 0$ for lower impact angles. Our experiments show that the splashing is suppressed in the upstream direction $\phi = \pi$ for $\theta = 45^\circ$ (see Fig. 2c). This case is predicted by our model, while the Hao model anticipates splash. We would like to point out, however, that $\beta = 0.14$ is obtained by taking the average of multiple experiments where the splashing threshold varied between $0.1 < \beta < 0.16$; therefore, a modest uncertainty is present in this threshold [1]. In accordance with the analytical results on the lamella velocity, it can be shown that our model predicts a strong and continuous suppression of splash for $\theta < 30$, eventually causing another impact outcome, which would lead to deposition or rebound. Previous experiments observed a total and partial rebound for $\theta < 10^\circ$ [6, 4], which supports our predictions.
To calculate the diameters and velocities of the secondary droplets after the lamella ejection T_e, Riboux & Gordillo [21] extended their RG model by taking into account the effects of the viscous shear force at the spreading rim. This friction force decreases the velocity and increases the thickness of the rim over time. We assume that the dimensionless azimuthal distribution (Eq. 5) is not being affected by the viscous shear force; therefore, we modified the evolution equations consequently as follows:

$$h_a^+ = \frac{h_{dist} h_a}{(1 - \sqrt{2}/\sqrt{\mathrm{Re} v_a h_a})} \quad \text{and} \quad v_a^+ = v_a(1 - \sqrt{2}/\sqrt{\mathrm{Re} v_a h_a}) \tag{7a,b}$$

with $h_a = h_l/3$ and $v_a = 2v_t$. Because the secondary droplets are ejected directly from the lamella, their size and velocity can be approximated as $d_{model} \approx h_a^+ D$ and $u_{model} \approx v_a^+ U/2$.

Results and discussion

Fig. 5a shows the size distribution of the secondary droplets detected at $\phi = 0$ and $\phi = \pi$. Our measurements show that the droplet size clearly changes in the azimuthal direction ϕ by changing the impact angle θ. While smaller droplets are present at $\phi = \pi$, larger droplets are detected at $\phi = 0$. This difference increases by decreasing θ. Nevertheless, the largest droplets generated on both sides ($\phi = 0$ and $\phi = \pi$) remained similar and $\sim 3\%$ of D. We would like to mention that the smallest size detected ($d_{sec} \approx 36$ µm) is restricted by the camera resolution limit; thus, it is likely that even smaller droplets are generated but cannot be detected by our system. The arithmetic mean size of the measured droplets is $d_{sec} \approx 52$ µm. To compute this value using the RG model, the elapsed time for the generation of secondary droplets must be known. For this, we referred to the study of Thoroddsen et al. [22], who observed that the majority of the secondary droplets are generated until $T_{max} \leq 100$ µs. The application of Eq. 7 from T_e to T_{max} gives us the approximated range of droplets generated. By taking the average of this range, the model predicts a mean diameter of $d_{model} = 49$ µm, which is in excellent agreement with our measurements.

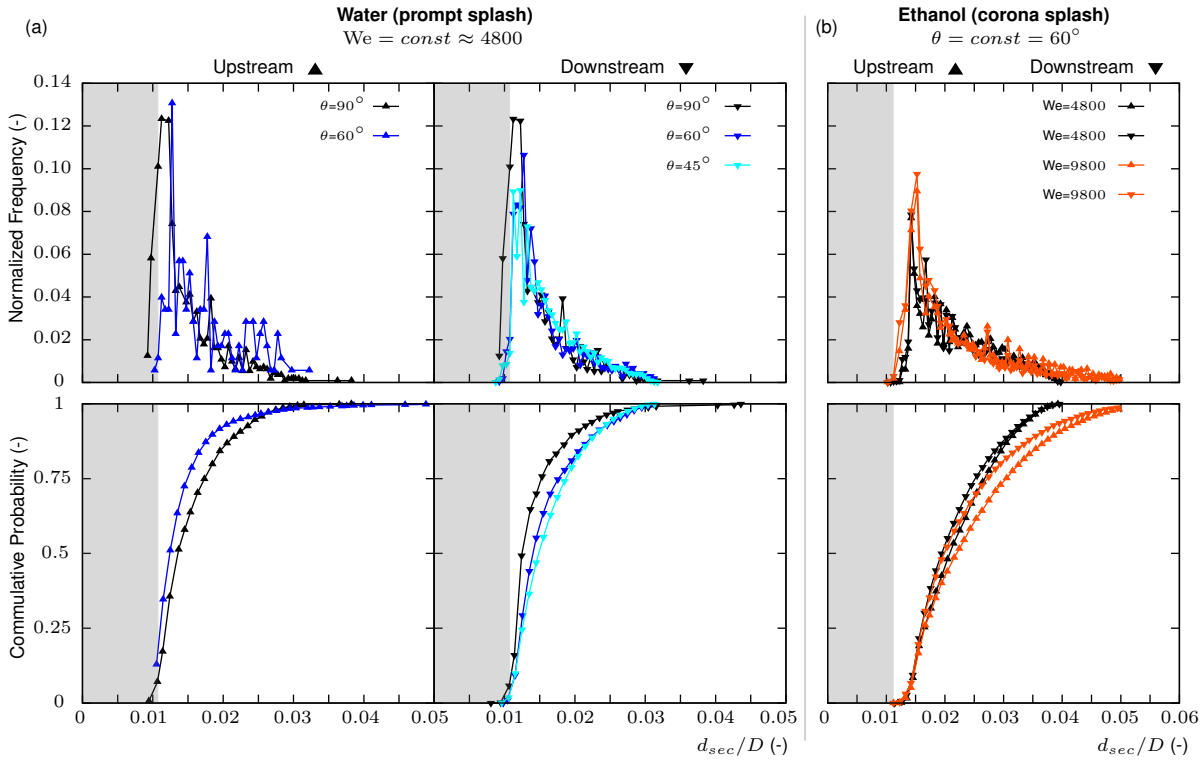

Figure 5. The size of the secondary droplets at $\phi = \pi$ (upstream) and $\phi = 0$ (downstream). The top diagrams show the histograms of the detected droplets; the bottom ones show the corresponding cumulative sums. (a) demonstrates the effect of the impact angle on the droplet size distribution. (b) shows the effect of the impact velocity on droplet size distribution for ethanol droplets. Gray area indicates diameters below the camera resolution limit.

https://doi.org/10.24355/dbbs.084-201909121447-0

Fig. 5b reveals the different and complex physical effects that are involved in the corona splashing regime. The most outstanding difference compared to the prompt splash is that at high We the droplets are generated due to two instabilities: rim instability and lamella breakup [23, 24]. When the corona is formed, its breakup generates larger droplets than the ones ejected from the rim; therefore, the size distribution is shifted, and the mean size diameter increases. This behavior has been previously observed by Mundo et al. [23]. By increasing the impact velocity, the ejected lamella becomes even bigger, generating larger droplets, although the droplets ejected from the rim are smaller [25]. Our measurements also show that larger droplets were generated at $\phi = \pi$ than $\phi = 0$. The reason for this is the short field of view of our recording system, which did not allow a full tracking on the lamella breakup at $\phi = 0$. The breakup mechanism at $\phi = \pi$ was always recorded due to early rupture of the lamella, therefore, more larger droplets were detected (see Fig. 2e). By zooming out, we could capture the entire breakup, but the new rough resolution did not allow us to measure the smallest droplet ejected from the rim. This illustrates the challenges that arise when attempting to measure the entire size scale of the secondary droplets.
By measuring the velocity of each secondary droplet, we observed that a certain droplet size does not necessarily coincide with a certain velocity. In fact, this velocity variation increases the smaller the droplets, making its prediction even more demanding. Similar results were obtained by Samenfink et al. [26] and Roisman et al. [24] in their investigations of the spray impact outcome. Fig. 6 shows the velocity magnitude average of droplet size clusters as a function of the droplet size. The average is taken to visualize and compare the experimental results in a compact way. A slight offset between the mean velocities can be observed for the water droplet impact; however, the standard deviation is so large ($\bar{u}/U \pm 2$) that the data obtained for the other angles θ are found within the uncertainty. In the corona splashing regime, the mean values collapsed into $\bar{u}/U \approx 1.8$ independently of the impact velocity (see Fig. 6b). These observations allow us also to conclude that the average droplet velocity is independent of the impact angle. These results support our theoretical approach.

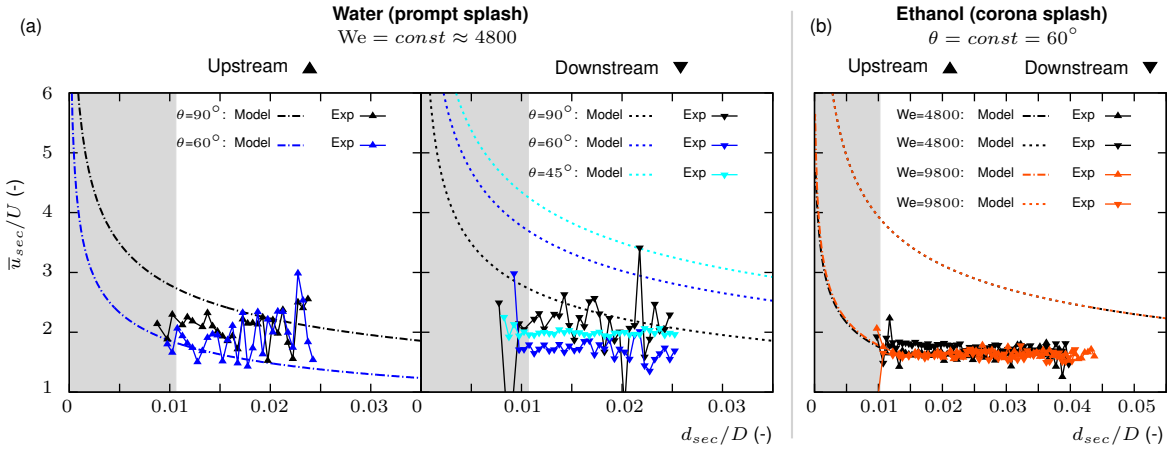

Figure 6. The velocity magnitude average for different droplet sizes. (a) demonstrates the effect of the impact angle on the secondary droplet velocity. (b) shows the effect of the impact velocity on the velocity of secondary droplets for ethanol droplets. The standard deviation of each marker decreases by increasing the droplet diameter from ± 2 to ± 0.5. The lines represent our approach for $\phi = \pi$ (dash-dotted) and $\phi = \pi$ (dashed). Gray area indicates the diameters below the camera resolution limit.

Fig.6 also shows a reasonable agreement of the model (Eq. 7b) with our measurements. Notice that the model describes only the ejection velocity at the rim, while we measured the droplets some microseconds after its ejection. Between this ejection and the measurement of different aerodynamics forces are acting on the droplets, reducing their velocity. This would explain why the RG model tends to overestimate the velocity of the droplets.

Conclusions

We investigated the impact of droplets on oblique surfaces at high Weber numbers analytically and experimentally. Our measurements show that the prompt and corona splashing generate different outcomes, suggesting that both phenomena must be considered separately. The threshold proposed by Roisman et al. [13] that indicates prompt splash when $\mathrm{Oh} < 0.0044$ is in agreement with our observations. This threshold provides simple discrimination at high impact velocity, which is difficult to achieve using only the theory of Riboux & Gordillo [1]. Nonetheless, we have demonstrated how useful this theory is in the description of the splashing outcome. Our results support the idea that the splashing occurs when the lift force imparted by the surrounding gas upon the lamella is greater than the capillary retraction force. In accordance with this model, we proposed a new approach to handle the oblique impact based on studies on the lamella formed by impinging jets. This approach can be used to estimate for the first time the splashing behavior in the azimuthal direction. We also demonstrated that using our approach the model gave an acceptable estimation of the secondary droplet size and velocity. Finally, we have shown that the impact angle mainly affects the shape and droplet size distribution, while the mean droplet velocity remains constant in the azimuthal direction for all studied cases. This conclusion is in conformity with both theoretical and experimental results.

https://doi.org/10.24355/dbbs.084-201909121447-0

Acknowledgements
We thank Rolf Radespiel for inspiring us to study the oblique impact of round jets, Patrick Loster for conducting part of the experiments, and the Deutsche Forschungsgemeinschaft DFG for the financial support (grant no. BA 4953-3).

Nomenclature

c	constants
d_{model}	secondary droplet diameter predicted [m]
d_{sec}	secondary droplet diameter [m]
D	primary droplet diameter [m]
F_L	lift force per unit length [N/m]
h_a	dimensionless lamella thickness at its root [-]
h_a^+	dimensionless lamella thickness at its root after consideration of the viscous shear force [-]
h_{dist}	dimensionless lamella thickness distribution [-]
h_l	dimensionless lamella thickness [-]
H_l	lamella thickness [m]
K_{lub}	lubrication force coefficient [-]
K_u	suction force coefficient [-]
Oh	Ohnesorge number [-]
p_0	atmospheric pressure [Pa]
p_l	lamella pressure [Pa]
R	primary droplet radius [m]
R_a	roughness average [m]
Re	Reynolds number [-]
R_z	roughness mean peak to valley height [m]
t_e	dimensionless ejection time [-]
T_0	temperature [°C]
T_e	ejection time of the lamella [s]
T_{max}	maximal ejection time of the secondary droplets [s]
u_a	dimensionless lamella velocity at its root [-]
u_a^+	dimensionless lamella velocity at its root after consideration of the viscous shear force [-]
u_l	dimensionless lamella velocity [-]
u_{model}	secondary droplet velocity predicted [m/s]
u_{sec}	secondary droplet velocity [m/s]
U	impact velocity [m/s]
U_l	lamella velocity [m/s]
U_n	normal impact velocity [m/s]
U_t	tangential impact velocity [m/s]
We	Weber number [-]
β	splashing parameter [-]
θ	impact angle [rad]
μ_g	gas dynamic viscosity [Pas]
μ_{liq}	liquid dynamic viscosity [Pas]
ρ_g	gas density [kg/m^3]
ρ_{liq}	liquid density [kg/m^3]
$\sigma_{liq,g}$	surface tension between liquid and gas [N/m]
ϕ	azimuthal angle [rad]
ω	angular velocity [rad/s]

References

[1] Riboux, G., and Gordillo, J.M., 2014, *Physical Review Letters*, 113 (2), 024507.
[2] Josserand, C., and Thoroddsen, S., 2016, *Annu. Rev. Fluid Mech.*, 48, 365.
[3] National Transportation Safety Board, 2016, *Aircraft Accident Report NTSB/AAR-16/01*, Washington, DC, USA.
[4] Li, H., 2013, Ph.D. thesis, Technische Universität Darmstadt.
[5] Courbin, L., Bird, J.C., and Stone, H.A., 2006, *Chaos: An Interdisciplinary Journal of Nonlinear Science*, 16(4), 041102.
[6] Šikalo, Š., Tropea, C., and Ganić, E.N., 2005,*Journal of Colloid and Interface Science*, 286(2), pp.661-669.
[7] Yeong, Y.H., Burton, J., Loth, E., and Bayer, I.S., 2014, *Langmuir*, 30(40), pp.12027-12038.
[8] Hao, J., Lu, J., Lee, L., Wu, Z., Hu, G., and Floryan, J.M., 2019, *Physical Review Letters*, 122 (5), 054501.
[9] Aboud, D.G., and Kietzig, A.M., 2015, *Langmuir*, 31(36), pp.10100-10111.
[10] Faßmann, B.W., Bansmer, S.E., Möller, T.J., Radespiel, R., and Hartmann, M., 2013, *Experiments in Fluids*, 54(5), 1516.
[11] Rein, M., 1993, *Fluid Dynamics Research*, 12(2), pp.61-93.

https://doi.org/10.24355/dbbs.084-201909121447-0

[12] Burzynski, D.A., and Bansmer, S.E., 2018, In *New Results in Numerical and Experimental Fluid Mechanics XI*, pp.511-521.
[13] Roisman, I.V., Lembach, A., and Tropea, C., 2015, *Advances in Colloid and Interface Science*, 222, pp.615-621.
[14] Palacios, J., Hernández, J., Gómez, P., Zanzi, C., and López, J., 2013, *Experimental Thermal and Fluid Science*, 44, pp.571-582.
[15] Bird, J.C., Tsai, S.S., and Stone, H.A., 2009, *New Journal of Physics*, 11(6), 063017.
[16] Zen, T.S., Chou, F.C., and Ma, J.L., 2010, *International Communications in Heat and Mass Transfer*, 37(8), pp.1025-1030.
[17] Schach, W., 1934, *Archive of Applied Mechanics*, 5(4), pp.245-265.
[18] Hasson, D., and Peck, R.E., 1964, *AIChE Journal*, 10(5), pp.752-754.
[19] Taylor, G., 1966, *Philosophical Transactions for the Royal Society of London. Series A, Mathematical and Physical Sciences*, pp.96-100.
[20] Povarov, O.A., Nazarov, O.I., Ignat'evskaya, L.A., and Nikol'Skii, A.I., 1976, *Journal of Engineering Physics and Thermophysics*, 31(6), pp.1453-1456.
[21] Riboux, G., and Gordillo, J.M., 2015, *Journal of Fluid Mechanics*, 772, pp.630-648.
[22] Thoroddsen, S.T., Takehara, K., and Etoh, T.G., 2012,*Journal of Fluid Mechanics*, 706, pp.560-570.
[23] Mundo, C.H.R., Sommerfeld, M., and Tropea, C., 1995, *International Journal of Multiphase Flow*, 21(2), pp.151-173.
[24] Roisman, I.V., Horvat, K., and Tropea, C., 2006, *Physics of Fluids*, 18(10), 102104.
[25] Yarin, A.L. and Weiss, D.A., 1995, *Journal of Fluid Mechanics*, 283, pp.141-173.
[26] Samenfink, W., Elsäßer, A., Dullenkopf, K., and Wittig, S., 1999, *International journal of heat and fluid flow*, 20(5), pp.462-469.

https://doi.org/10.24355/dbbs.084-201909121447-0